Improved quarter-point crack tip element

L.J. Gray [a], A.-V. Phan [a], Glaucio H. Paulino [b,*], T. Kaplan [a]

[a] *Computer Science and Mathematics Division, Oak Ridge National Laboratory, Oak Ridge, TN 37831-6367, USA*
[b] *Department of Civil and Environmental Engineering, University of Illinois, Urbana-Champaign, 205 North Mathews Avenue, 2209 Newmark Laboratory, Urbana, IL 61801-2352, USA*

Abstract

We present a modification to the quarter-point crack tip element and employ this element in two-dimensional boundary integral fracture analysis. The standard singular element is adjusted so that the near-tip crack opening displacement satisfies a known constraint: the coefficient of the term which is linear in the distance to the tip must vanish. Stress intensity factors calculated with the displacement correlation technique are shown to be highly accurate, and significantly more accurate than with the standard element. The improvements are especially dramatic for mixed-mode problems involving curved and interacting cracks.
© 2002 Published by Elsevier Science Ltd.

Keywords: Fracture mechanics; Stress intensity factors; Quarter-point element; Boundary integral analysis

1. Introduction

The numerical modeling of crack stability and propagation [18] requires the accurate determination of stress intensity factors (SIFs), which in turn relies on the correct representation of the local crack tip stress and displacement fields. For a crack geometry, Williams [23,24] result for the displacement $\mathbf{u} = u_k$, $k = 1, 2$, in the neighborhood of the tip is

$$u_k(r, \theta) = a_k + b_k(\theta)r^{1/2} + c_k(\theta)r + d_k(\theta)r^{3/2} + \cdots, \tag{1}$$

where r, θ are the distance to, and the direction emanating from, the tip, respectively. Thus the crack opening displacement (COD) $\Delta \mathbf{u} = \Delta u_k$, $k = 1, 2$ at the tip, is

$$\Delta u_k(r, \theta) = b_k(\theta)r^{1/2} + c_k(\theta)r + d_k(\theta)r^{3/2} + \cdots. \tag{2}$$

In both finite and boundary element modeling of discrete cracks, the standard approach consists of incorporating the critical $\sqrt{r}$ behavior by means of the 'quarter-point' (QP) element originally developed by Henshell and Shaw [12], and Barsoum [2]. Use of special elements at the crack tip has significantly

---

improved the accuracy of SIF calculations [3,16,21], and the original QP element has been extended and refined in a number of ways [1,14,15]. Nevertheless, in either finite or boundary element analyses, the prediction of sliding and twisting stress intensity modes, K_{II}, K_{III}, has not been nearly as accurate as for the opening mode K_I.

Recently, Gray and Paulino [10] proved that, irrespective of the problem geometry or boundary conditions, the series expansion in Eq. (2) must have $c_k = 0$ for $\Delta \mathbf{u}$ *on the crack surface* (for related work see [17]). As will be discussed below, in general the QP element fails to satisfy this constraint, and it is this flaw that is addressed in this paper. By forcing the linear term in $\Delta \mathbf{u}$ to be zero, we expect to have a more accurate analysis in the tip region. This is in fact borne out by the test calculations, as a dramatic improvement in the accuracy of SIFs is seen. These calculations employ a symmetric-Galerkin boundary integral fracture analysis (see, for example, [5,20]) coupled with a displacement correlation technique (DCT) for evaluating the SIFs.

The remaining sections of this paper are organized as follows. The next section presents the shape functions for the improved QP element. The symmetric-Galerkin boundary integral approximation for modeling generic fracture mechanics problems, to be used in the computational examples, is reviewed in Section 3. The numerical examples in Section 4 treat several different crack configurations, and display the superiority of the modified QP element over the standard element. Finally, some closing remarks are given in Section 5.

2. Modified quarter-point element

The two-dimensional QP element is based upon the three-noded quadratic element. For $t \in [0, 1]$, the shape functions for this element are given by

$$\begin{aligned}
\psi_1(t) &= (1-t)(1-2t), \\
\psi_2(t) &= 4t(1-t), \\
\psi_3(t) &= t(2t-1).
\end{aligned} \tag{3}$$

As $\Delta u = 0$ at the crack tip, assumed to be at $t = 0$, the representations of the crack tip geometry and COD are

$$\Gamma(t) = \sum_{j=1}^{3} \left(x_j \psi_j(t), y_j \psi_j(t) \right),$$

$$\Delta u_k(t) = \sum_{j=2}^{3} \left(\Delta u_1^j \psi_j(t), \Delta u_2^j \psi_j(t) \right). \tag{4}$$

Here (x_j, y_j) are the coordinates of the three nodes defining the element, and Δu_k^j the nodal values of the COD.

Henshell and Shaw [12] and independently Barsoum [2], demonstrated that by moving the mid-node coordinates (x_2, y_2) three fourths of the way towards the tip, the parameter t becomes $(r/L)^{1/2}$, with L being the distance from (x_1, y_1) to (x_3, y_3). As a consequence, the leading order term in Δu_k^j at $t = 0$, which is t, is the correct square root of distance. Note however, that the next term, which is t^2, is r/L. According to Gray and Paulino [10], this term should vanish, and the modification presented below replaces this term with $(r/L)^{3/2}$.

For the new approximation, we keep the representation of $\Gamma(t)$ as in Eq. (4), so that the property $t \approx \sqrt{r}$ remains, and the interpolation of the geometry remains quadratic. However for the COD, we define new shape functions by adding a cubic term:
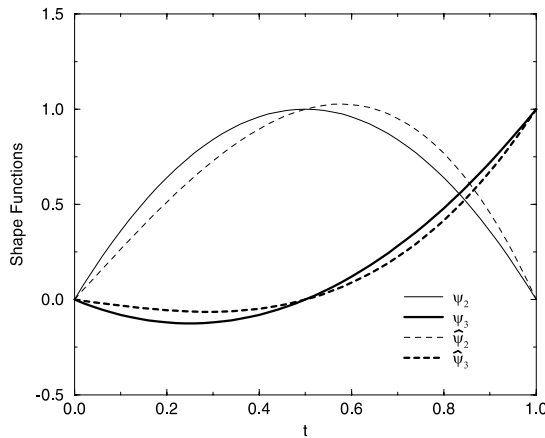
Fig. 1. Standard (ψ_2, ψ_3) and modified ($\widehat{\psi}_2, \widehat{\psi}_3$) shape functions.

$$\widehat{\psi}_2(t) = 4t(1-t) - 4t(1-t)(1-2t)/3 = -\tfrac{8}{3}(t^3 - t),$$
$$\widehat{\psi}_3(t) = t(2t-1) + 2t(1-t)(1-2t)/3 = \tfrac{4}{3}(4t^3 - t). \tag{5}$$

This additional contribution accomplishes the cancellation of the $t^2 \approx r$ term, without disturbing the interpolation, i.e.,

$$\widehat{\psi}_2(0) = 0, \quad \widehat{\psi}_2(1/2) = 1, \quad \widehat{\psi}_2(1) = 0, \tag{6}$$

$$\widehat{\psi}_3(0) = 0, \quad \widehat{\psi}_3(1/2) = 0, \quad \widehat{\psi}_3(1) = 1. \tag{7}$$

As might be expected, this alteration does not radically alter the COD shape functions, as seen in Fig. 1.

3. Symmetric-Galerkin boundary integral fracture analysis

The test calculations reported below employ a two-dimensional symmetric-Galerkin approximation, and thus this section presents a quick overview of this technique. A good introduction to the Galerkin method is provided in the recent text by Bonnet [4], and a recent review by Bonnet et al. [5] on symmetric-Galerkin provides an excellent summary and references to the literature. The primary motivation for this brief review is to point out that, in the Galerkin approach, the shape functions do more than simply define the interpolation approximations for the surface and boundary functions: they are directly involved in how the continuous integral equations are reduced to finite matrices. Thus, in this approach, the change from the standard quater-point element to the new one will significantly impact the approximation.

The two-dimensional displacement boundary integral equation is given by [7,19]

$$\mathscr{U}(P) = u_k(P) + \int_{\partial B} T_{kj}(P,Q)u_j(Q)\,\mathrm{d}Q - \int_{\partial B} U_{kj}(P,Q)\tau_j(Q)\,\mathrm{d}Q = 0, \tag{8}$$

where $\mathbf{u}$ and $\boldsymbol{\tau}$ denote displacement and traction, respectively. As customary, the kernel functions $T_{kj}(P,Q)$ and $U_{kj}(P,Q)$ are given by the Kelvin solution for a point load in an infinite medium (formulas for these functions, along with those for the stress equation below, can be found in the Appendix A). The corresponding integral equation for the surface stress is essential for treating crack geometries, and in the symmetric-Galerkin approach it is this equation that is employed on the crack surface. The stress equation

(from which one gets an equation for surface traction by multiplying by the appropriate normal vector) is obtained by differentiating Eq. (8) with respect to P, resulting in

$$\mathscr{S}(P) = \sigma_{lk}(P) + \int_{\partial B} S_{lkm}(P,Q)u_m(Q)\,\mathrm{d}Q - \int_{\partial B} D_{lkm}(P,Q)\tau_m(Q)\,\mathrm{d}Q = 0. \tag{9}$$

In a Galerkin formulation, the above integral equations are enforced 'on average', in the form

$$\int_{\partial B} \psi_l(P)\mathscr{U}(P)\,\mathrm{d}P = 0,$$
$$\int_{\partial B} \psi_l(P)\mathscr{S}(P)\,\mathrm{d}P = 0. \tag{10}$$

The weight functions $\psi_l(P)$ are the shape functions employed to interpolate the boundary displacements and tractions. Again, note that the modified shape functions for the QP are employed to define the Galerkin equations in the crack tip region.

For symmetric-Galerkin, the displacement equation is employed on the part of the boundary where displacement is specified, while the traction equation is employed on the part of the boundary where traction is known. As the name implies, this results in a symmetric coefficient matrix. This remains true for fracture problems, with the proviso that the unknowns on the crack surface are now the jump in displacement.

A key advantage of the Galerkin approach is that the extra boundary integration simplifies the task of defining and evaluating the hypersingular integral. Nevertheless, the main computational task in implementing Eq. (10) is the evaluation of the singular integrals. For two-dimensional problems there are a number of techniques available, e.g., [13,8]. In this work, the singular integration is accomplished by means of direct hybrid analytical/numerical algorithms, as described by Gray [9].

In regards to the singular integration, it is important to note that the modified shape functions present no difficulties, and in fact are easily incorporated in an existing quadratic element code. The standard quadratic and modified QP shape functions can be conveniently written in the general form

$$\widehat{\psi}_j(t) = \psi_j(t) + \alpha\beta_j t(1-t)(1-2t). \tag{11}$$

Here α is used to distinguish a crack tip element ($\alpha = 1$) from a regular element ($\alpha = 0$); the values for the constants β are $\beta_1 = \beta_3 = \pm 2/3$ and $\beta_2 = \mp 4/3$, and the upper or lower sign is employed if the crack tip is located at the first ($t = 0$) or third node ($t = 1$), respectively. In the latter case, by letting $s = 1 - t$, one again obtains the modified shape functions in Eq. (5) in terms of the variable s.

From this form it is clear that implementing the modified crack tip only requires the additional integration of the $t(1-t)(1-2t)$ expression. As this function is zero at the three nodes, it only contributes to the "lower order" singular terms, and in these terms it simply changes some polynomial coefficients. Thus, the analytical integration codes built for the standard quadratic shape functions [9] can be re-used here with only minor modification.

4. Test calculations

SIFs provided by the QP elements (both modified and standard) will be calculated by means of the DCT. The point here is to assess the quality of the modified QP element by means of a very simple method such as the DCT. The general expression of SIFs by means of the DCT technique are given by

$$K_{\mathrm{I}} = \frac{G}{\kappa+1} \lim_{r\to 0} \sqrt{\frac{2\pi}{r}} \Delta u_2,$$

$$K_{\mathrm{II}} = \frac{G}{\kappa+1} \lim_{r\to 0} \sqrt{\frac{2\pi}{r}} \Delta u_1, \tag{12}$$

where Δu_k is the COD in the coordinate system associated with the crack tip under consideration, G is shear modulus, and v is Poisson's ratio,

$$\kappa = 3 - 4v \text{ (plane strain)}, \quad \kappa = \frac{3-v}{1+v} \text{ (plane stress)}. \tag{13}$$

By using the modified QP shape functions in Eq. (5), one gets (the crack tip is assumed to be at the first node A, see the schematic of parameter space in Fig. 2)

$$\Delta u_k = \Delta u_k^{\mathrm{B}} \widehat{\psi}_2(t) + \Delta u_k^{\mathrm{C}} \widehat{\psi}_3(t)$$
$$= \tfrac{1}{3}(8\Delta u_k^{\mathrm{B}} - \Delta u_k^{\mathrm{C}})t + \tfrac{4}{3}(\Delta u_k^{\mathrm{C}} - 2\Delta u_k^{\mathrm{B}})t^3. \tag{14}$$

Use of (14) in (12), with $t = \sqrt{r/L}$, yields

$$K_{\mathrm{I}} = \frac{G}{3(\kappa+1)} \sqrt{\frac{2\pi}{L}} (8\Delta u_2^{\mathrm{B}} - \Delta u_2^{\mathrm{C}}),$$

$$K_{\mathrm{II}} = \frac{G}{3(\kappa+1)} \sqrt{\frac{2\pi}{L}} (8\Delta u_1^{\mathrm{B}} - \Delta u_1^{\mathrm{C}}). \tag{15}$$

Thus, SIFs are given directly in terms of the nodal values of the COD at the crack tip element.
In order to assess the various features of the modified QP element, the following examples are presented:

1. Single interior crack
   1.1. Mode-I case
   1.2. Mixed-mode case
2. Pair of interacting collinear cracks
3. Pair of interacting circular-arc cracks
4. 'Off-center' crack
5. Three-point bending specimen.

In the presentation below, the modified QP is compared with the standard QP element. For all examples, consistent units are used and the following material constants are employed: Young's modulus $E = 0.36$, Poisson's ratio $v = 0.27$. The first three examples deal with infinite body problems and the numerical results
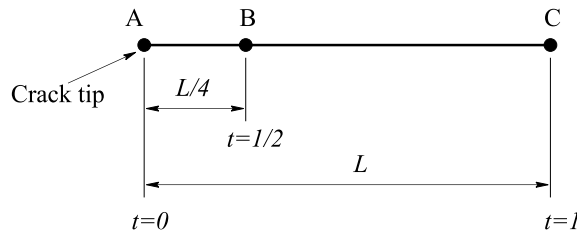

Fig. 2. Crack tip element.

are compared with the analytical solutions given by Tada et al. [22], whereas the last two examples involve finite body cases.

4.1. Single interior crack

Consider a plate containing a single interior crack which is oriented arbitrarily with respect to the angle θ, as illustrated by Fig. 3. The plate is subjected to the remote uniaxial tension $\sigma = 100$ applied along the y-axis. The crack length is $2a = 0.4$ and the plate dimensions are $2H = 2W = 200$ which can be approximated as an unbounded domain in this case. Two cases are considered, the mode-I case ($\theta = 0$), and the mixed-mode case ($0 < \theta < \pi/2$).

4.1.1. Mode-I case ($\theta = 0$)

Consider a single interior crack aligned along the x-axis, i.e. $\theta = 0$ (see Fig. 3). The CODs (displacement discontinuities along the crack) Δu_2 are depicted in Fig. 4 with the crack being discretized into 10 uniform quadratic elements. It can be seen that the SG-BEM solutions using the standard and modified QP elements are in very good agreement with the analytical solution.

With this mesh, however, while the modified QP element can give very accurate value of the mode-I SIF ($K_I/K_I^{exact} = 0.9999$), the result obtained from the standard QP element is ($K_I/K_I^{exact} = 1.0233$). A finer mesh needs to be employed in the standard QP case to improve the result while the solution obtained from the modified QP case is mostly insensitive with the mesh (see Table 1). In fact, when the modified QP shape functions are used, the solution is slightly less accurate as the mesh becomes finer. This may be explained by the fact that the crack tip element should be 'long enough' in order for the t^3 terms in the shape functions (see Eqs. (5) and (14)) to exhibit their presence. This is another advantage of the modified QP element because it means that the mesh on the crack does not need to be excessively refined in order to obtain accurate results.
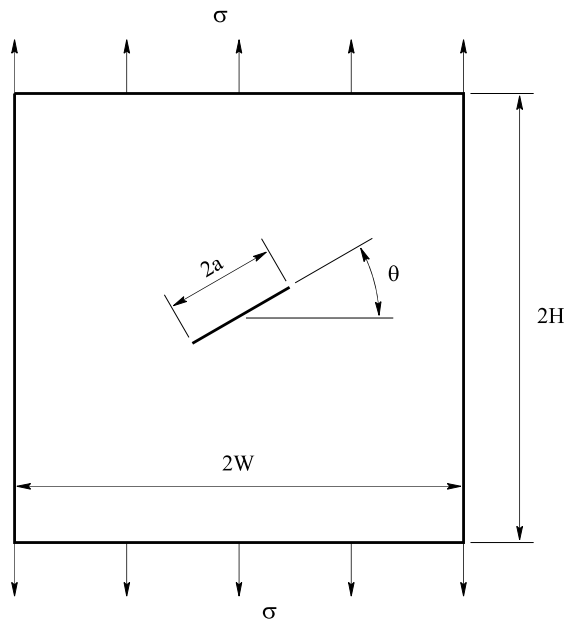

Fig. 3. Single interior crack.
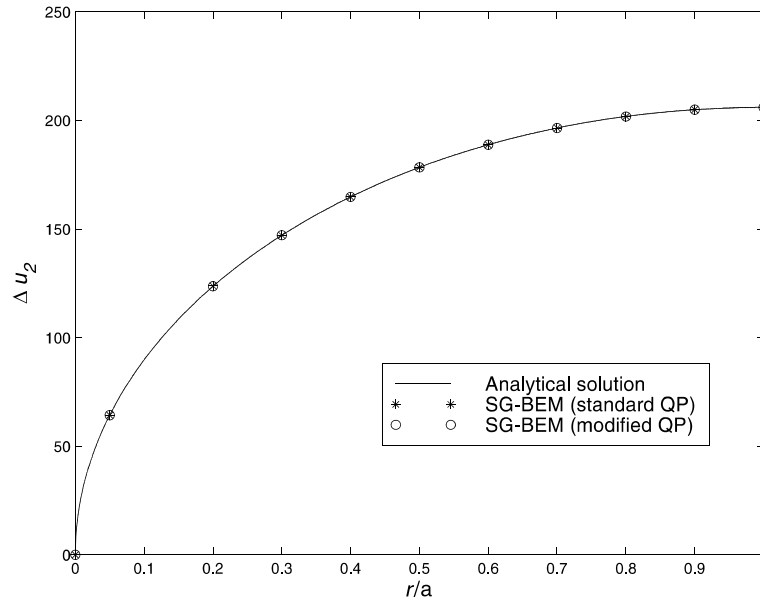
Fig. 4. COD solutions.

Table 1
K_I/K_I^{exact} as function of the number of crack elements

# Crack elements	Standard QP	Modified QP
8	1.0298	1.0002
10	1.0233	0.9999
20	1.0110	0.9996
30	1.0070	0.9996
40	1.0050	0.9995
50	1.0038	0.9995
60	1.0030	0.9995
70	1.0025	0.9995
80	1.0021	0.9995

4.1.2. Mixed-mode case $(0 < \theta < \pi/2)$

Consider mixed-mode situation where $0 < \theta < \pi/2$. Table 2 reveals that the errors of K_I and K_{II} evaluated from the standard and modified QP elements are consistent and uniform no matter what value of θ. Again, with 10 crack elements employed, modified QP shape functions give excellent accuracy for both K_I and K_{II}.

4.2. Pair of interacting collinear cracks

This is an example of two interacting cracks which have the same length $2a = 0.2$ and are separated by a gap b (see Fig. 5). The plate can be considered as an infinite domain by using the same dimensions as those in the previous example. The cracks are subjected to uniaxial tension $\sigma = 100$ applied in the direction perpendicular to the cracks. The mode-I SIF at the inner crack tips is of interest.

Table 2
Normalized SIFs as functions of angle θ

Angle θ	Standard QP		Modified QP	
	$K_{\mathrm{I}}/K_{\mathrm{I}}^{\mathrm{exact}}$	$K_{\mathrm{II}}/K_{\mathrm{II}}^{\mathrm{exact}}$	$K_{\mathrm{I}}/K_{\mathrm{I}}^{\mathrm{exact}}$	$K_{\mathrm{II}}/K_{\mathrm{II}}^{\mathrm{exact}}$
$\pi/12$	1.0233	1.0233	0.9999	0.9999
$\pi/6$	1.0233	1.0233	0.9999	0.9999
$\pi/4$	1.0233	1.0233	0.9999	0.9999
$\pi/3$	1.0233	1.0233	0.9999	0.9999
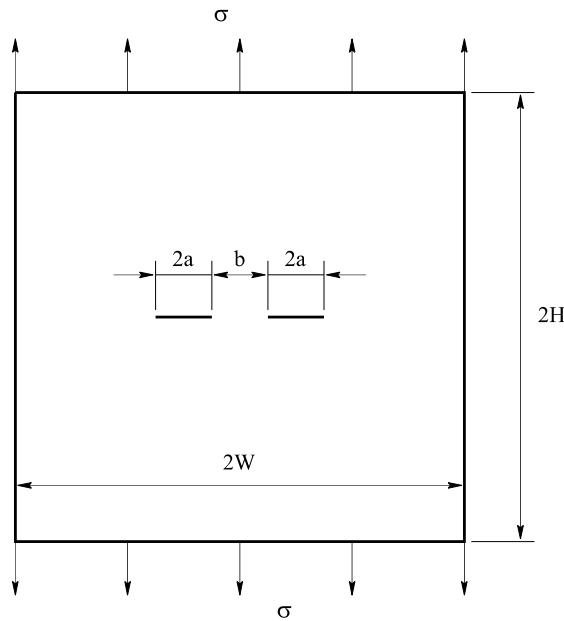
Fig. 5. Pair of interacting collinear cracks.

For the case $b = 4a$, the numerical results for $(K_{\mathrm{I}}/K_{\mathrm{I}}^{\mathrm{exact}})$, as a function of the number of elements per crack, are virtually the same as for the central crack example. The same remarks as above therefore apply here. The effect of crack interaction is depicted in Fig. 6 where 10 elements per crack are employed. The numerical error of K_{I} increases as the gap between the cracks decreases. However, it can be seen that the increase in error rate for the standard QP is higher as the cracks come closer to each other. Moreover, the error from the modified QP is always much lower no matter what the value of the gap. This error is less than 1% even when the ratio b/a is less than one-quarter.

4.3. Pair of interacting circular-arc cracks

It is generally recognized that the DCT combined with the standard QP shape functions usually produce poor accuracy for SIFs in case of mixed-mode situations. Use of modified QP elements instead can improve considerably this accuracy as shown in this example.

Consider a mixed-mode example through a pair of circular-arc cracks of radius $R = 0.1$, angle $\theta = \pi/2$, embedded in a plate of dimension $(2H \times 2W)$, and subjected to remote biaxial tension σ as shown in Fig. 7.
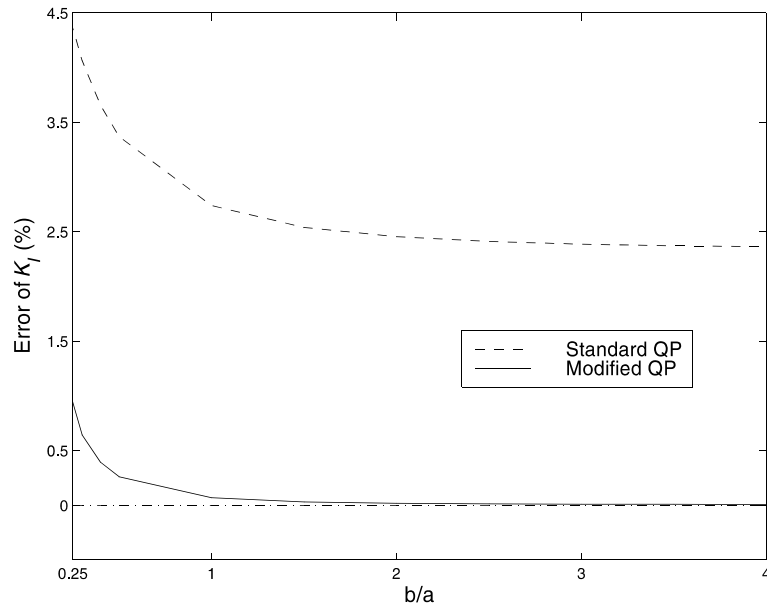
Fig. 6. Effect of crack interaction.
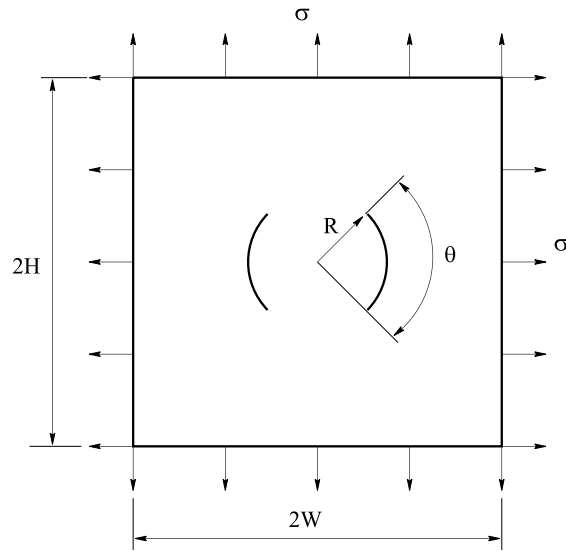
Fig. 7. Pair of circular-arc cracks.

The same plate dimension as in two previous examples is chosen again in order to consider this problem as an unbounded domain. Five elements (of uniform length) per crack are used. For comparison purposes, an asymptotic solution for the COD, valid as $r \to 0$, can be derived from the exact SIF values,
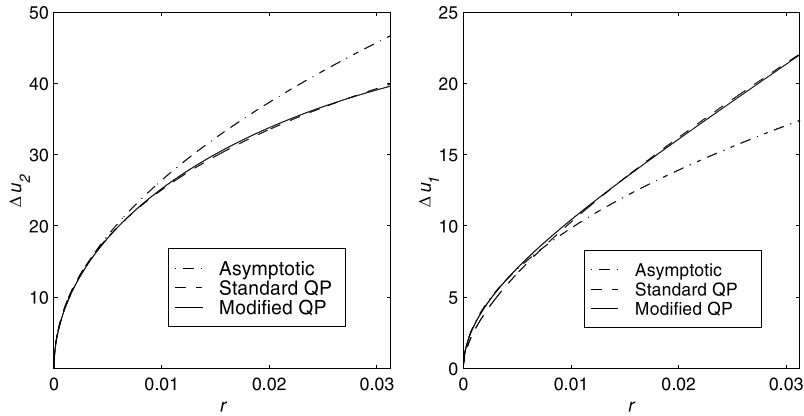
Fig. 8. Solutions for the COD $\Delta\mathbf{u}$ along the crack tip element.

Table 3
Normalized SIFs

Normalized SIFs	Standard QP	Modified QP
K_I/K_I^{exact}	1.0711	1.0047
K_{II}/K_{II}^{exact}	0.7512	0.9625

$$\Delta u_2^{asy} = \frac{\kappa+1}{G}\sqrt{\frac{r}{2\pi}}K_I^{exact},$$
$$\Delta u_1^{asy} = \frac{\kappa+1}{G}\sqrt{\frac{r}{2\pi}}K_{II}^{exact}. \quad (16)$$

Fig. 8 illustrates the SG-BEM result versus the asymptotic solution for the CODs Δu_2 and Δu_1 along the crack tip element.

Although Δu_2 given by the standard and modified QP are seen to be in very good agreement with Δu_2^{asy} near the crack tip as shown in the left plot of Fig. 8, the accuracy of the K_I obtained from the modified QP is much better as shown in Table 3. On the other hand, while Δu_1 given by the modified QP is in good agreement with the asymptotic solution, this is not the case for Δu_1 obtained from the standard QP (see the right plot of Fig. 8). This explains why the K_{II} from the modified QP is much more accurate than that from the standard one as seen in Table 3.

The effect of crack interaction on the SIFs for modes I and II (as a function of θ) is depicted in Fig. 9. For mode-I SIF, similar remarks as those derived in the pair of aligned cracks can also be observed here. However, while the mode-II SIF obtained from the standard QP is mostly unchanged with the increase of θ, the modified QP element helps to dramatically improve this quantity, even where the crack tips are very close ($\theta \approx \pi$).

4.4. 'Off-center' crack

This example deals with mixed-mode case in a finite body. Consider a crack whose location and orientation are arbitrary in a plate, subjected to the remote uniaxial tension σ applied along the y-axis as shown in Fig. 10. The following geometry data are studied: $2W = 2H = 2$, $2a = 0.5$ and $e_x = e_y = 0.5$. The
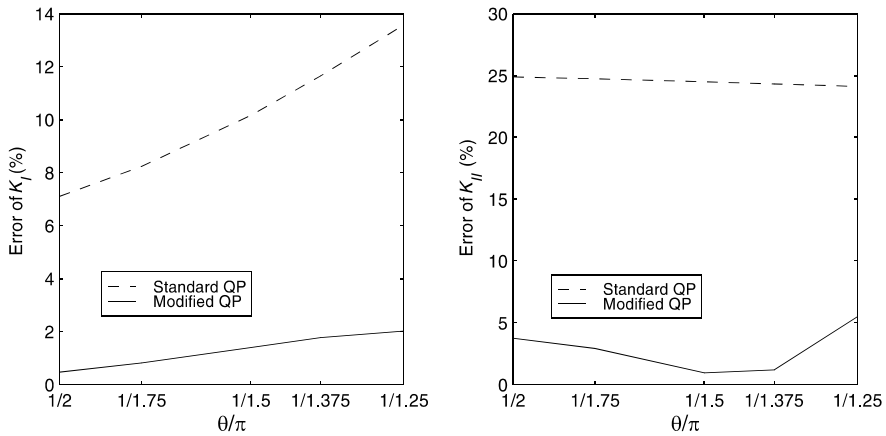
Fig. 9. Effect of crack interaction on SIFs.
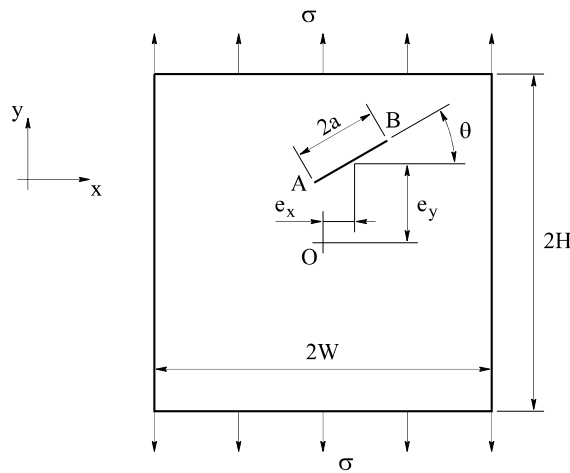
Fig. 10. 'Off-center' crack.

standard and modified QP shape functions are used with 10 uniform elements on the crack. Numerical results, normalized by $\sigma(\pi a)^{1/2}$, for mode-I and -II SIFs at both crack tips A and B are presented in Tables 4 and 5 along with those given in [25]. It can be observed that all the solutions obtained from the modified QP shape functions are much closer to the reference than those from the standard ones. Note that the reference results are not the exact solution because they are also obtained by another numerical approach. However, since the approach used is the boundary collocation method which is supposed to be more accurate than the DCT, it can be concluded once again that mixed-mode SIFs are improved by using the modified QP shape functions. Finally, these improved results are illustrated in Fig. 11 as functions of angle θ.

4.5. Three-point bending specimen

The last example deals with a surface crack and bending deformation. A three-point bending beam under opening mode is shown in Fig. 12 is studied. Mode-I SIF is evaluated for a wide range of geometry of

Table 4
Normalized SIFs at crack tip A as functions of crack angle θ

Angle θ	$K_{\mathrm{I}}^{\mathrm{A}}/\sigma\sqrt{\pi a}$			$K_{\mathrm{II}}^{\mathrm{A}}/\sigma\sqrt{\pi a}$		
	Standard QP	Modified QP	Reference [25]	Standard QP	Modified QP	Reference [25]
0	1.2259	1.2022	1.2001	0.0306	0.0274	0.0271
$\pi/6$	0.9096	0.8926	0.8918	0.4977	0.4869	0.4870
$\pi/3$	0.3097	0.3034	0.3030	0.4842	0.4743	0.4738
$\pi/2$	0.0000	0.0000	0.0000	0.0000	0.0000	0.0000
$2\pi/3$	0.2807	0.2767	0.2764	−0.5004	−0.4891	−0.4873
$5\pi/6$	0.8987	0.8819	0.8794	−0.5328	−0.5189	−0.5154
π	1.2540	1.2278	1.2227	−0.0469	−0.0436	−0.0426

Table 5
Normalized SIFs at crack tip B as functions of crack angle θ

Angle θ	$K_{\mathrm{I}}^{\mathrm{B}}/\sigma\sqrt{\pi a}$			$K_{\mathrm{II}}^{\mathrm{B}}/\sigma\sqrt{\pi a}$		
	Standard QP	Modified QP	Reference [25]	Standard QP	Modified QP	Reference [25]
0	1.2540	1.2278	1.2227	−0.0469	−0.0436	−0.0426
$\pi/6$	0.9665	0.9460	0.9431	0.4950	0.4844	0.4832
$\pi/3$	0.3178	0.3109	0.3086	0.5067	0.4953	0.4933
$\pi/2$	0.0000	0.0000	0.0000	0.0000	0.0000	0.0000
$2\pi/3$	0.3347	0.3254	0.3217	−0.4918	−0.4816	−0.4790
$5\pi/6$	0.9527	0.9315	0.9274	−0.4646	−0.4577	−0.4580
π	1.2259	1.2022	1.2001	0.0306	0.0274	0.0271
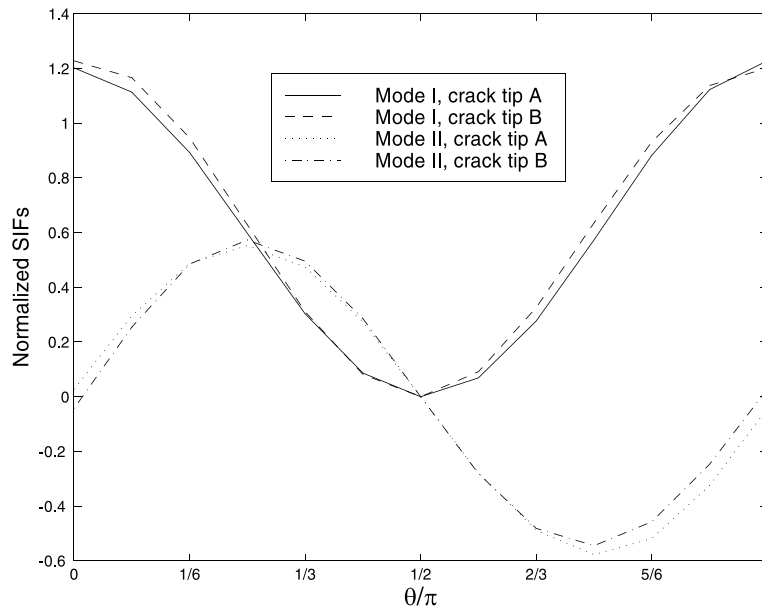
Fig. 11. Normalized SIFs as functions of angle θ.
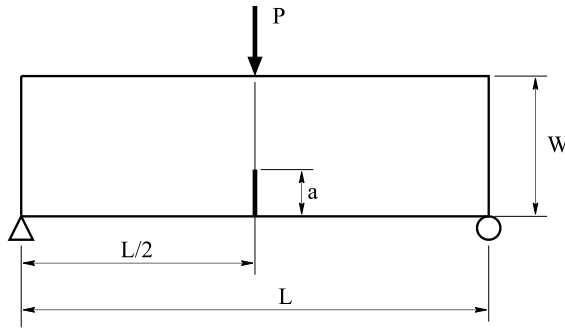
Fig. 12. Three-point bending specimen.

Table 6
$K_{\mathrm{I}}/K_{\mathrm{I}}^{\mathrm{ref}}$ as functions of L/W and a/W

a/W	$L/W = 2.5$		$L/W = 8$	
	Standard QP	Modified QP	Standard QP	Modified QP
0.1	0.9898	0.9870	1.0020	0.9981
0.2	0.9816	0.9855	0.9959	0.9995
0.3	0.9800	0.9868	0.9941	1.0011
0.4	0.9797	0.9887	0.9914	1.0011
0.5	0.9791	0.9905	0.9868	0.9990
0.6	0.9770	0.9916	0.9791	0.9946
0.7	0.9722	0.9920	0.9657	0.9862
0.8	0.9610	0.9908	0.9546	0.9851

the beam and crack using crack elements of uniform length $\Delta a = 0.02W$. The SG-BEM results are listed in Table 6 and compared with the analytical solution proposed by Guinea et al. [11] (Fig. 13). Deviation of the standard and modified QP results from the reference is illustrated in Fig. 13. It can be seen that all results obtained from the modified QP shape functions are in better agreement with the reference except in case
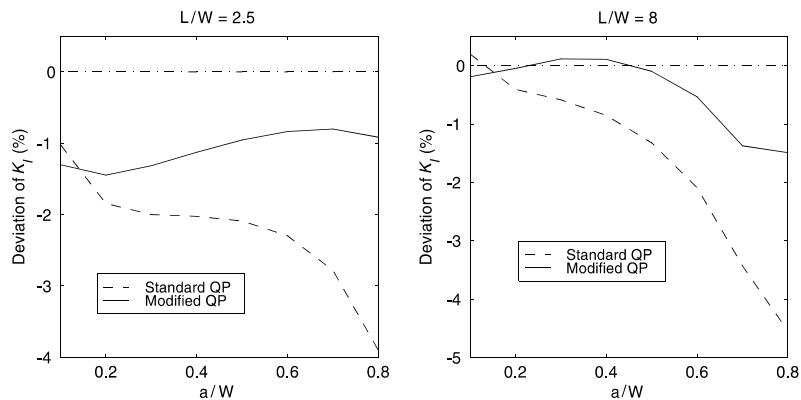

Fig. 13. Deviation of the standard and modified QP results from the reference [11].

$L/W = 2.5$ and $a/W = 0.1$. Since the Guinea et al.'s solution is a good but not an absolutely exact reference, this incompatibility might serve as an indication to revise the proposed expression in the above case.

5. Conclusions

The modified QP crack tip element defined in this paper has been shown to produce highly accurate SIFs. This is the case even though the calculations employed relatively coarse meshes, combined with the very simple *local* method (displacement correlation); to calculate SIFs. Moreover, the modified QP element has been shown to be consistently superior to the standard QP element. Thus, this improved element should be very useful for crack propagation simulations, as in these calculations is difficult to minutely control the meshing.

As the modified element only serves to improve the local COD solution at the tip, it is not expected to have a significant impact on non-local SIF evaluation methods, e.g., *J*-integral. However, the hope is that combining this element with simple and computationally inexpensive local SIF methods will produce sufficient accuracy, in both two and three dimensions.

The extension of this work to three dimensions should be possible. The first step would be to establish that the linear term constraint remains valid; extending the two-dimensional analysis in [10] appears to be straightforward. The second step, developing a modified crack tip element (again from quadratic to cubic), should follow along the same lines as presented herein. These investigations are currently being pursued by the authors.

Acknowledgements

Appendix A

For convenience, the kernel functions for the displacement and stress boundary integral equations are provided below. The Kelvin solution U_{kj} is well known to be

$$U_{kj}(P,Q) = \frac{1}{8\pi G(1-v)}\left[-(3-4v)\delta_{kj}\log(r) + r_{,k}r_{,j}\right]. \tag{A.1}$$

Differentiating this displacement to obtain traction results in

$$T_{kj}(P,Q) = -\frac{1}{4\pi(1-v)r}\left[\left\{(1-2v)\delta_{kj} + 2r_{,k}r_{,j}\right\}\frac{\partial r}{\partial n} - (1-2v)\left\{n_j r_{,k} - n_k r_{,j}\right\}\right]. \tag{A.2}$$

The kernels $D_{lkm}(P,Q)$ (singular) and $S_{lkm}(P,Q)$ (hypersingular) for the stress equation are given by (see [6], Eqs. (5.69) and (5.70))

$$D_{lkm} = \frac{1}{4\pi(1-v)r}[(1-2v)\{\delta_{lm}r_{,k} + \delta_{km}r_{,l} - \delta_{lk}r_{,m}\} + 2r_{,l}r_{,k}r_{,m}]$$

$$S_{lkm} = \frac{G}{2\pi(1-v)r^2}\left[2\frac{\partial r}{\partial \mathbf{n}}(\{1-2v\}\delta_{lk}r_{,m} + v(\delta_{km}r_{,l} + \delta_{lm}r_{,k}) \right. \tag{A.3}$$
$$\left. - 4r_{,l}r_{,k}r_{,m}) + (1-2v)(2n_m r_{,l}r_{,k} + n_k\delta_{lm} + n_l\delta_{km}) \right.$$
$$\left. + 2v(n_l r_{,k}r_{,m} + n_k r_{,l}r_{,m}) - (1-4v)n_m\delta_{lk}\right].$$

In these equations, v is Poisson's ratio, G is shear modulus, δ_{ij} is the Kronecker delta, $r_{,i} = \partial r/\partial q_i$, and q_i is the ith coordinate of the field point Q.

References

[1] Banks-Sills L. Application of the finite element method to linear elastic fracture mechanics. Appl Mech Rev 1991;44:447–61.
[2] Barsoum RS. On the use of isoparametric finite elements in linear fracture mechanics. Int J Numer Meth Engng 1976;10:25–37.
[3] Blandford GE, Ingraffea AR, Liggett JA. Two-dimensional stress intensity factor computations using the boundary element method. Int J Numer Meth Engng 1981;17:387–404.
[4] Bonnet M. Boundary integral equation methods for solids and fluids. England: Wiley and Sons; 1995.
[5] Bonnet M, Maier G, Polizzotto C. Symmetric Galerkin boundary element method. ASME Appl Mech Rev 1998;51:669–704.
[6] Brebbia CA, Telles JCF, Wrobel LC. Boundary element techniques. Berlin and New York: Springer-Verlag; 1984.
[7] Cruse TA. Boundary element analysis in computational fracture mechanics. Boston: Kluwer Academic Publishers; 1988.
[8] Frangi A, Novati G. Symmetric BE method in two-dimensional elasticity: evaluation of double integrals for curved elements. Computat Mech 1996;19:58–68.
[9] Gray LJ. Evaluation of singular and hypersingular Galerkin boundary integrals: direct limits and symbolic computation. In: Sladek V, Sladek J, editors. Singular Integrals in the Boundary Element Method. Advances in Boundary Elements. Computational Mechanics Publishers; 1998. p. 33–84. [chapter 2].
[10] Gray LJ, Paulino GH. Crack tip interpolation, revisited. SIAM J Appl Math 1998;58:428–55.
[11] Guinea G, Pastor J, Planas J, Elices M. Stress intensity factor, compliance and CMOD for a general three-point-bend beam. Int J Fract 1998;89:103–16.
[12] Henshell RD, Shaw KG. Crack tip finite elements are unnecessary. Int J Numer Meth Engng 1975;9:495–507.
[13] Hölzer SM. How to deal with hypersingular integrals in the symmetric BEM. Commun Numer Meth Engng 1993;9:219–32.
[14] Horváth Á. Higher-order singular isoparametric elements for crack problems. Commun Numer Meth Engng 1994;10:73–80.
[15] Lim IL, Johnston IW, Choi SK. Application of singular quadratic distorted isoparametric elements in linear fracture mechanics. Int J Numer Meth Engng 1993;36:2473–99.
[16] Linkov AM, Mogilevskaya SG. Complex hypersingular integrals and integral equations in plane elasticity. Acta Mech 1994;105:189–205.
[17] Martin PA. End-point behavior of solutions to hypersingular equations. Proc R Soc London A 1991;432:301–20.
[18] Rice JR. Mathematical analysis in the mechanics of fracture. In: Liebowitz H, editor. Fracture—an advanced treatise, vol. II. Oxford: Pergamon Press; 1968. p. 191–311.
[19] Rizzo FJ. An integral equation approach to boundary value problems of classical elastostatics. Quart Appl Math 1967;25:83–95.
[20] Sirtori S, Maier G, Novati G, Miccoli S. A Galerkin symmetric boundary element method in elasticity: formulation and implementation. Int J Numer Meth Engng 1992;35:255–82.
[21] Sladek J, Sladek V. Dynamic stress intensity factors studied by boundary integro-differential equations. Int J Numer Meth Engng 1986;23:919–28.
[22] Tada H, Paris P, Irwin G. The stress analysis of cracks handbook. Hellertown, Pennsylvania: Del Research Corporation; 1973.
[23] Williams ML. Stress singularities resulting from various boundary conditions in angular corners of plates in extension. ASME J Appl Mech 1952;19:526–8.
[24] Williams ML. On the stress distribution at the base of a stationary crack. ASME J Appl Mech 1957;24:109–14.
[25] Yuanhan W. Asymmetric crack problems calculated by the boundary collocation method. Engng Fract Mech 1991;40:133–43.